Supplemental Material for

Teleseismic S-wave tomography of South Island, New Zealand upper mantle

Daniel W. Zietlow[1], Anne F. Sheehan[1], and Melissa V. Bernardino[1]

[1]Cooperative Institute for Research in Environmental Sciences (CIRES) and Department of Geological Sciences, University of Colorado, Boulder,

399 UCB, 2200 Colorado Ave., Boulder, CO 80309-0399

CONTENTS OF THIS FILE

Supplemental Table S1, Supplemental Figures S1 to S5, and derivation of crust and sediment corrections for travel-time data

INTRODUCTION

This supporting information provides a table of station locations and crust/sediment corrections made at those stations (Supplemental Table S1), as well as figures showing travel-time picks in the frequency band 0.08 – 0.12 Hz (Supplemental Figure S2), an L-curve test (Supplemental Figure S3), and a checkerboard test and model inversion from a ray-based code (Supplemental Figures S4 and S5). It also contains a derivation for the crust and sediment corrections made to the teleseismic travel-time measurements.

TABLES

STATION	LAT	LON	CRUST THICK (km)	SED THICK (km)	SED CORR (s)	CRUST CORR (s)	TOTAL CORR (s)
APZ*	-46.8334	167.9888	29.2	0	0.00	1.62	1.62
CASS	-43.0169	171.7265	29.6	0	0.00	1.64	1.64
CROE	-42.3365	171.3984	27.1	0	0.00	1.51	1.51
DCZ*	-45.4663	167.1535	52.7	0	0.00	2.93	2.93
DSZ	-41.7467	171.8045	30.3	0	0.00	1.68	1.68

EAZ	-45.2327	169.3082	38.4	0	0.00	2.13	2.13
FOZ	-43.5338	169.8154	33.6	0	0.00	1.87	1.87
FREW	-43.4537	171.9040	23.6	0	0.00	1.31	1.31
JCZ	-44.0749	168.7854	37.2	0	0.00	2.07	2.07
KELY	-42.2623	172.2204	32.1	0	0.00	1.78	1.78
KHZ*	-42.4160	173.5390	28.7	0	0.00	1.59	1.59
LBZ	-44.3872	170.1843	32.6	0	0.00	1.81	1.81
LTZ	-42.7833	172.2709	26.6	0	0.00	1.48	1.48
MLZ	-45.3682	168.1183	32.8	0	0.00	1.82	1.82
MQZ	-43.7077	172.6536	24.2	0	0.00	1.34	1.34
MSZ	-44.6750	167.9263	30.3	0	0.00	1.68	1.68
NNZ*	-41.2188	173.3793	37.6	0	0.00	2.09	2.09
NZ02*	-43.9980	166.5011	16.5	0.8	0.62	0.68	1.30
NZ03*	-43.0018	165.9995	14.6	0.78	0.61	0.60	1.20
NZ04*	-41.9993	165.5024	14.9	0.80	0.62	0.61	1.23
NZ05	-40.6493	167.2510	14.7	0.64	0.50	0.82	1.31
NZ06	-39.7498	168.0011	17.8	0.45	0.35	0.99	1.34
NZ07	-40.2501	169.0003	22.7	0.62	0.48	1.26	1.74
NZ08	-40.9998	168.5011	16.9	0.72	0.56	0.94	1.50
NZ09	-41.6507	167.8998	14.5	0.87	0.68	0.81	1.48
NZ10	-43.2007	168.0004	16.4	0.69	0.54	0.91	1.45
NZ11	-43.3000	168.8502	24.5	0.72	0.56	1.36	1.92
NZ12	-43.0017	169.5986	28.7	0.75	0.58	1.59	2.18
NZ13	-42.4997	169.0000	18.7	0.71	0.55	1.04	1.59
NZ14	-42.6506	169.9500	25.1	0.76	0.59	1.39	1.99
NZ15	-42.1506	170.3996	29.2	0.76	0.59	1.62	2.21
NZ16	-41.7499	169.2491	18.6	0.71	0.55	1.03	1.59
NZ18	-41.0002	170.0000	20.7	0.70	0.54	1.15	1.69
NZ19	-40.7502	170.9004	23.7	0.72	0.56	1.32	1.88
NZ20	-40.1995	170.7503	24.3	0.70	0.54	1.35	1.89
NZ21	-39.5005	170.0001	22.7	0.64	0.50	1.26	1.76
NZ22	-44.5006	173.9987	30.6	1.26	0.98	1.70	2.68
NZ23	-45.1494	174.8520	30.8	0.72	0.56	1.71	2.27
NZ24	-45.4984	176.0026	30.8	0.36	0.28	1.71	1.99

NZ25	-45.9978	174.7504	33.7	0.54	0.42	1.87	2.29
NZ26	-46.9979	174.4984	28.6	0.53	0.41	1.59	2.00
NZ27	-46.5007	173.2497	24.5	1.06	0.82	1.36	2.19
NZ28	-45.9639	171.7514	30.7	0.93	0.72	1.71	2.43
NZ29	-45.2474	172.2535	28.4	1.14	0.89	1.58	2.46
NZ30	-45.4980	173.5010	27.6	1.36	1.06	1.53	2.59
ODZ	-45.0456	170.6445	27.7	0	0.00	1.54	1.54
OPZ	-45.8860	170.5977	36.6	0	0.00	2.03	2.03
OXZ	-43.3259	172.0383	22.6	0	0.00	1.26	1.26
PYZ*	-46.1679	166.6807	37.1	0	0.00	2.06	2.06
QRZ	-40.8272	172.5290	32.3	0	0.00	1.79	1.79
RPZ	-43.7163	171.0538	28.9	0	0.00	1.61	1.61
SYZ	-46.5385	169.1388	33.6	0	0.00	1.87	1.87
THZ*	-41.7642	172.9051	37.4	0	0.00	2.08	2.08
TUZ	-45.9556	169.6311	35.8	0	0.00	1.99	1.99
WHZ	-45.8940	167.9470	27.6	0	0.00	1.53	1.53
WKZ	-44.8287	169.0175	42.8	0	0.00	2.38	2.38
WVZ	-43.0760	170.7366	30.2	0	0.00	1.68	1.68

Supplemental Table S1. List of station locations used in this study along with estimates of crust (crust thick) and sediment (sed thick) thicknesses used to make corrections to the travel-time data. The corrections shown here (sed corr, crust corr, and total corr) are for a vertically traveling S-wave assuming a sediment speed of 1.0 km/s, a crustal speed of 3.6 km/s, an oceanic crustal speed of 3.8 km/s (stations NZ02 – NZ04), and a mantle speed of 4.5 km/s. Starred stations (*) are stations at which Pn measurements were not published (Collins and Molnar, 2014) and we instead used crustal thicknesses from Salmon et al. (2013).

FIGURES

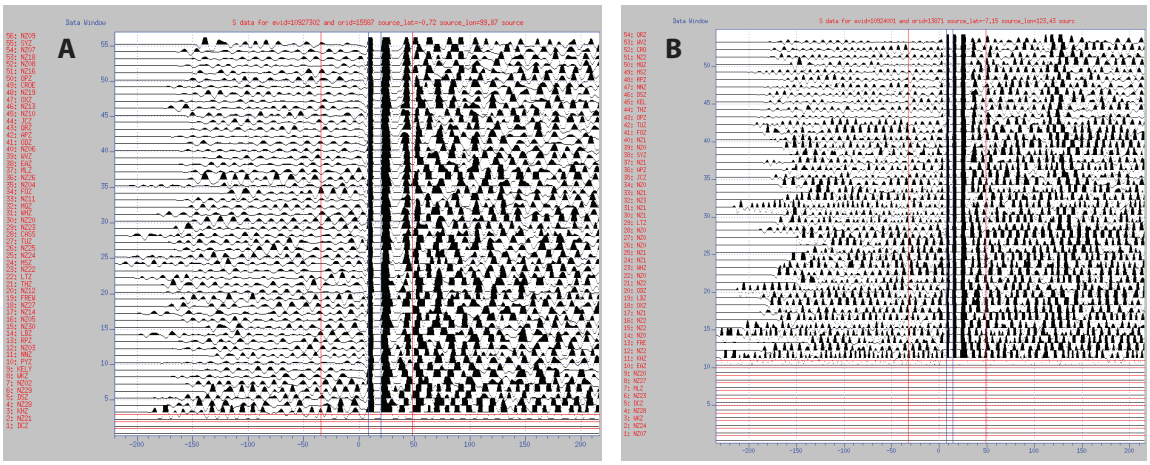

Supplemental Figure S1. Examples of the cross-correlation of waveforms. Waveforms of an earthquake A) from offshore Sumatra with backazimuth of 283° (m_b = 7.1) in the filter band 0.05 – 0.1 Hz; and B) from the Banda Sea with backazimuth of 297° (m_b = 6.3) in the filter band 0.08 – 0.12 Hz. Red lines denote the beam window and blue lines denote the robust window as defined in *dbxcor* (Pavlis and Vernon, 2010). Station names are to the left of the seismograms, with MOANA OBSs beginning in "NZ." The x-axis is time in seconds. Traces are ordered by correlation coefficient, with the trace with the highest correlation coefficient at the top.

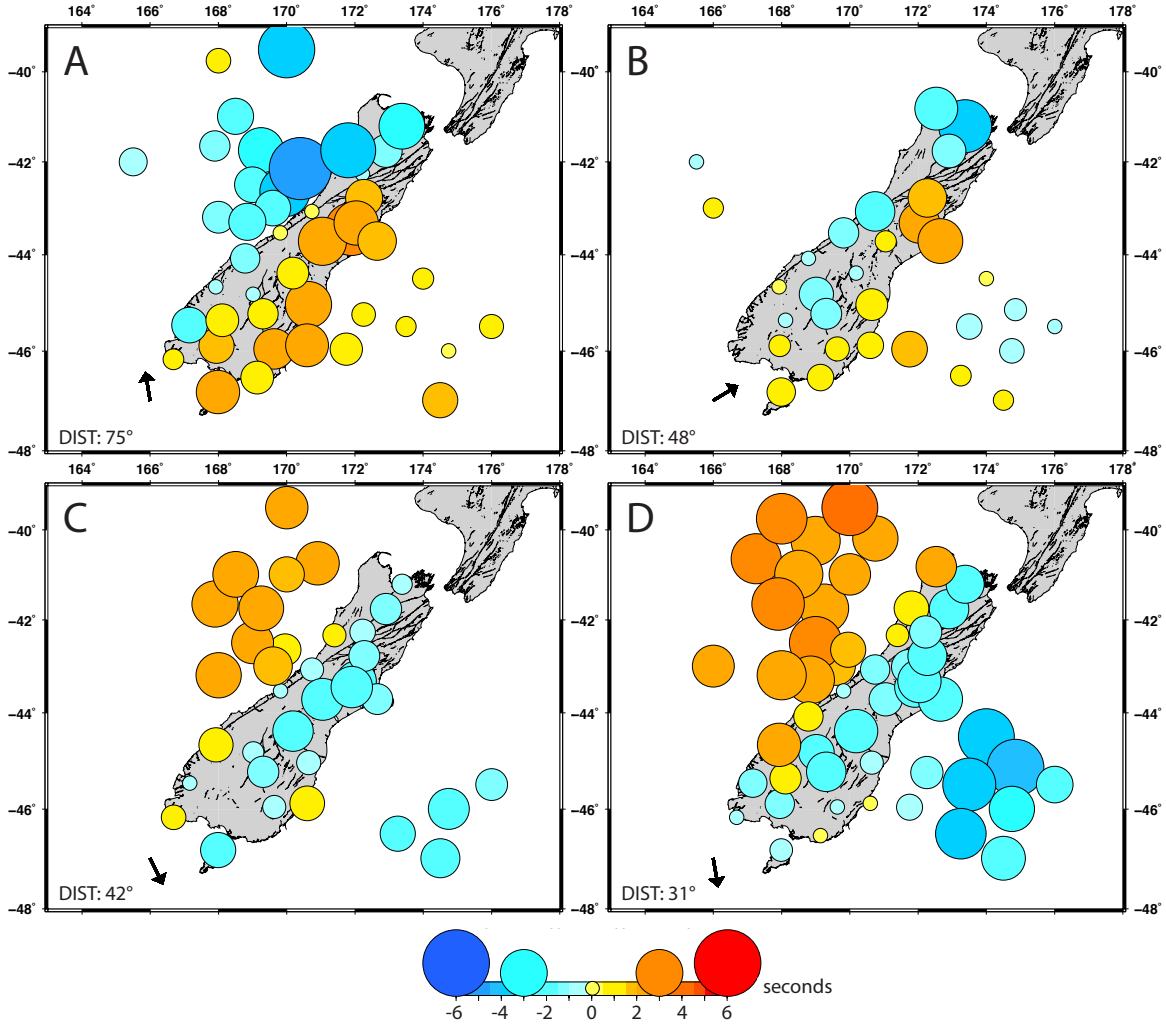

Supplemental Figure S2. Plot of measured travel-time residuals in the band 0.08 – 0.12 Hz after application of a crustal and sediment correction for 4 different events from different backazimuths. Earthquakes A) near the South Sandwich Islands with backazimuth of 171° (m_b = 6.2; B) on the Southweast Indian Ridge with a backazimuth of 239° (m_b = 5.8); C) offshore the Solomon Islands with a backazimuth of 334° (m_b = 6.3); and D) north of Vanuatu with a backazimuth of 350° (m_b = 5.7). Black arrows point from the earthquake, with epicentral distance given on the plot. A negative (positive) travel-time residual indicates an early (late) arrival with respect to average times for the AK135 reference model (Kennett et al., 1995).

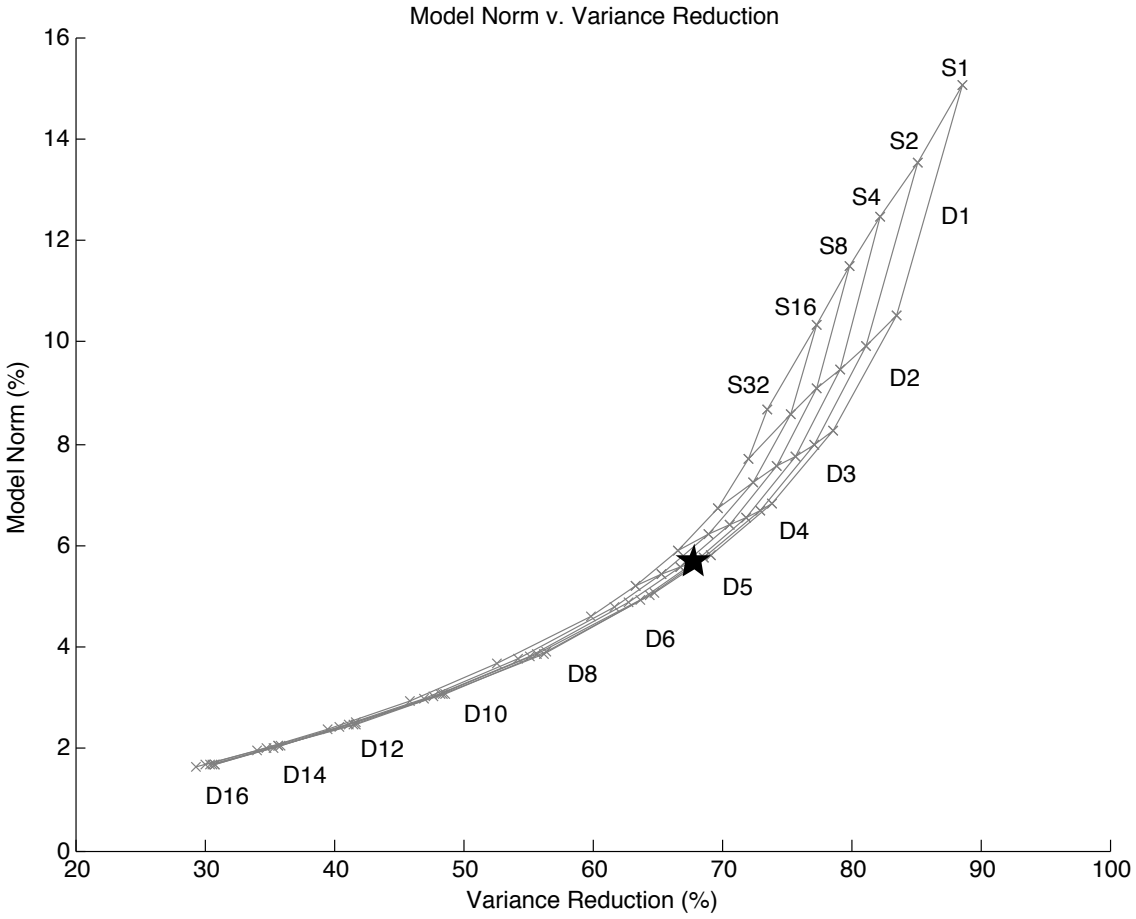

Supplemental Figure S3. Plot depicting the trade-off analysis between model norm and variance reduction for inversion of the crust and sediment corrected S-wave travel-time data. Each curve represents a single smoothing value (labeled "S"), and each point on the curve shows a damping value (labeled "D"). The black star shows the parameters used in this study (damping = 5 and smoothing = 4).

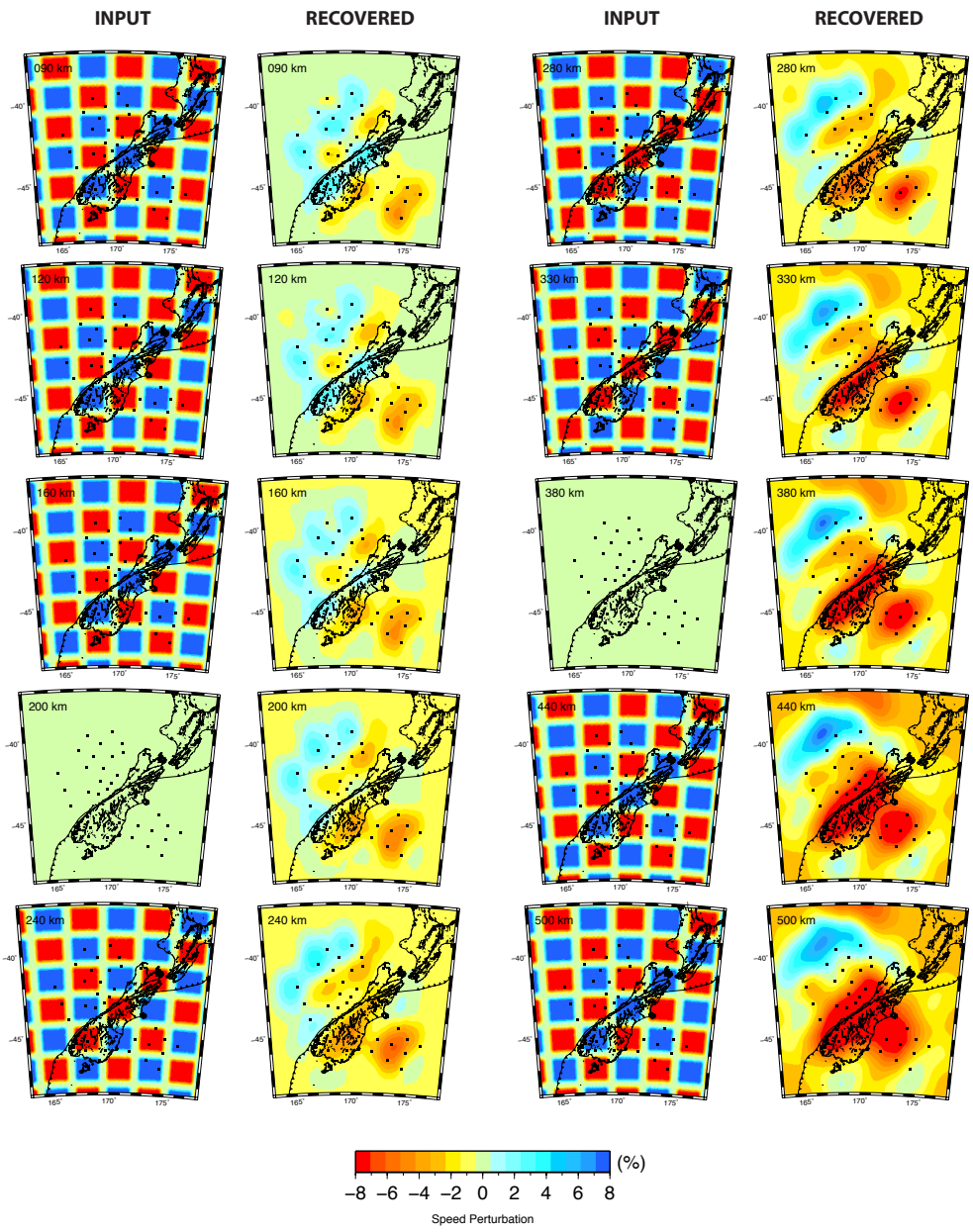

Supplemental Figure S4. Resolution for depth slices at 90, 120, 160, 200, 240, 280, 330, 380, 440, and 500 km based on a standard checkerboard test with cubes 200 km per side using the ray-based code from Roecker et al. (2006). The left column shows the synthetic input structure (+8% or -8% the reference S-wave speed of AK135) and the right column shows the recovered structure.

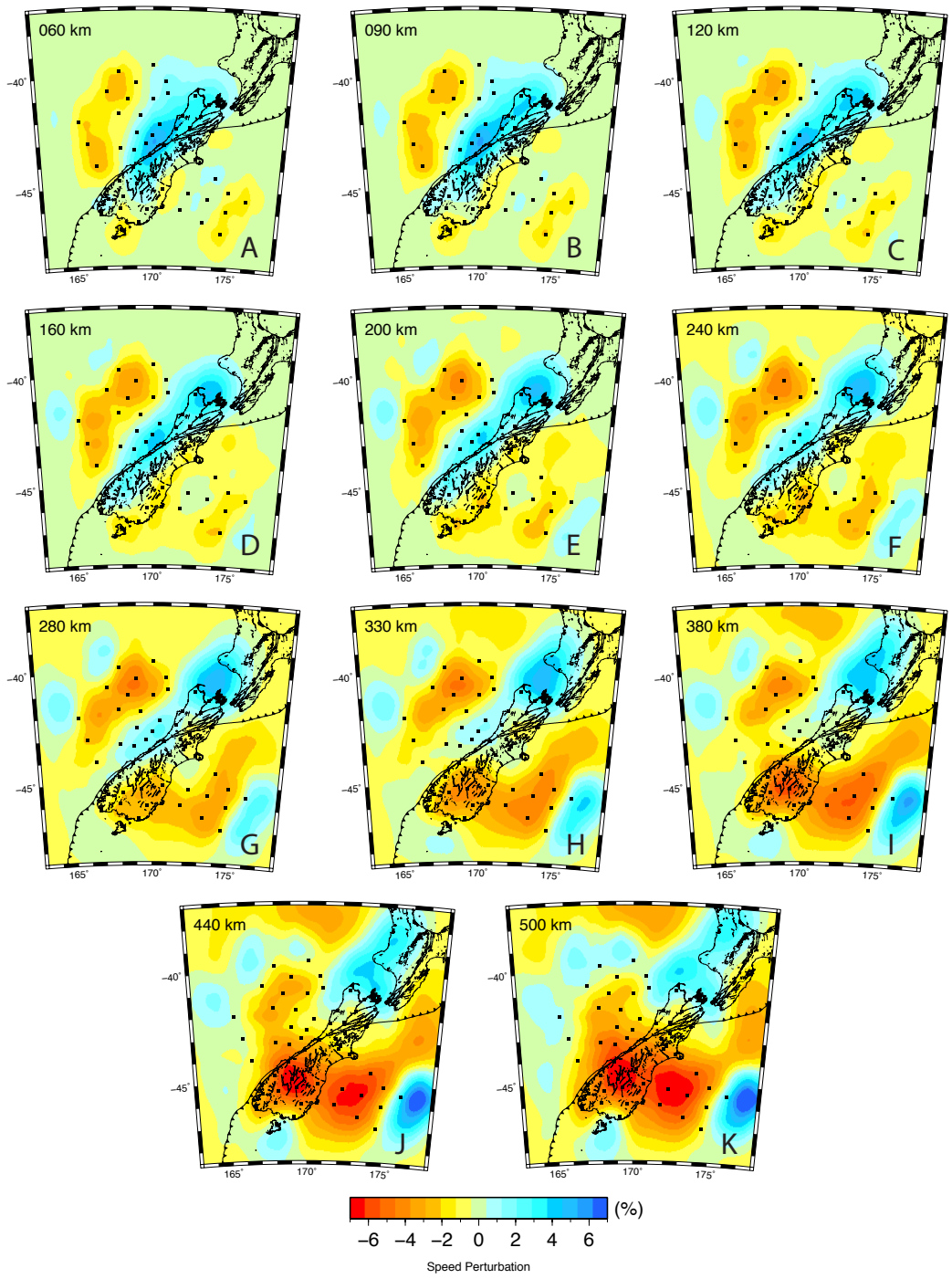

Supplemental Figure S5. Depth slices at 60, 90, 120, 160, 200, 240, 280, 330, 380, 440, and 500 km through an S-wave tomogram obtained using the ray-based tomography code of Roecker et al. (2006), using the stations shown in Figure 1 and earthquakes shown in Figure 3.

CORRECTIONS FOR SEDIMENT AND CRUST DERIVATION

` We assume that the sediment and crust correction to the teleseismic travel-time measurements is the sum of the travel-time difference between a ray traveling in sediment versus mantle plus the difference between a ray traveling in crust versus mantle (see schematic below).

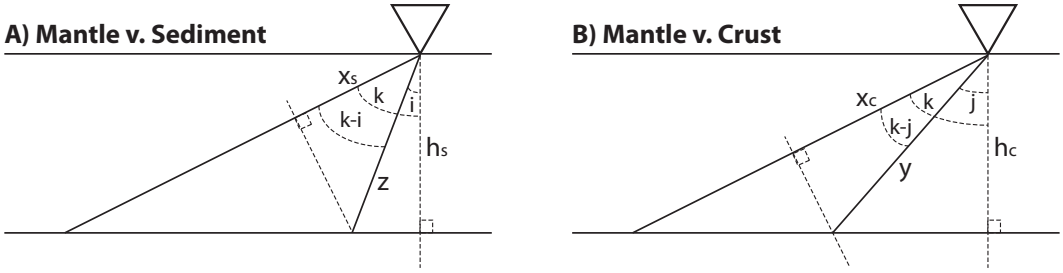

The travel-time through the sediment layer is

$$t_c = \frac{h_s}{v_s \cos(i)}\,, \tag{S1}$$

where h_s is the thickness of the sediment, v_s is the wave speed in sediment, and i is the incidence angle in the sediment. For the equivalent path through the mantle:

$$x_s = z\cos(k-i)\,, \tag{S2}$$

where k is the incidence angle in the mantle and $z = h_s / cos(i)$. The time it takes to travel path x_s is

$$t_m = \frac{h_s \cos(k-i)}{v_m \cos(i)}\,, \tag{S3}$$

where v_m is the wave speed in the mantle. The difference in travel-time between a ray traveling in sediment versus in the crust is

$$\Delta T_s = \frac{h_s}{\cos(i)}\left[\frac{1}{v_s} - \frac{\cos(k-i)}{v_m}\right]. \tag{S4}$$

Likewise, for the travel-time difference between crust and mantle:

$$\Delta T_c = \frac{h_c}{\cos(j)}\left[\frac{1}{v_c} - \frac{\cos(k-j)}{v_m}\right]. \tag{S5}$$

Thus, the total correction is

$$\Delta T = \frac{h_s}{\cos(i)}\left[\frac{1}{v_s} - \frac{\cos(k-i)}{v_m}\right] + \frac{h_c}{\cos(j)}\left[\frac{1}{v_c} - \frac{\cos(k-j)}{v_m}\right]. \quad \text{(S6)}$$

Equation S6 is the same as Equation 1 in the main text.

FILE OF S-WAVE TOMOGRAM

A comma-separated values file of the S-wave tomogram is provided (S_TOMO_data.csv). It is in the format Longitude (°), Latitude (°), Depth (km), dVs (%), Hit Quality.

REFERENCES CITED

Collins, J.A. and Molnar, P., 2014, Pn anisotropy beneath the South Island of New Zealand and implications for distributed deformation in continental lithosphere: J. Geophys. Res. Solid Earth, vol. 119, doi:10.1002/2014JB011233.

Kennett, B.L.N., Engdahl, E.R., and Buland, R., 1995, Constraints on seismic velocities in the Earth from traveltimes: Geophys. J. Int., vol. 122, p. 108-124, doi:10.1111/j.1365-246X.1995.tb03540.

Pavlis, G.L., and Vernon, F.L., 2010, Array processing of teleseismic body waves with the USArray: Computers & Geosciences, vol. 36, p. 910-920, doi:10.1016/j.cageo.2009.10.008.

Roecker, S., Thurber, C., Roberts, K., and Powell, L., 2006, Refining the image of the San Andreas Fault near Parkfield, California using a finite difference travel time computation technique: Tectonophysics, vol. 426, p. 189-205, doi:10.1016/j.tecto.2006.02.026.

Salmon, M., Kennett, B., Stern, T., and Aitken, A., 2013, The Moho in Australia and New Zealand: Tectonophysics, vol. 609, p. 288-298, doi: 10.1016/j.tecto.2012.07.009.